STELLARATOR NONLINEARLY SATURATED PERIODICITY-BREAKING IDEAL MAGNETOHYDRODYNAMIC EQUILIBRIUM STATES

W.A. Cooper[1], D. López-Bruna[2], M.A. Ochando[2], F. Castejón[2], J.P. Graves[3], A. Kleiner[3], S. Lanthaler[3], H. Patten[3], M. Raghunathan[3] and J.M. Faustin[4]

[1]Swiss Alps Fusion Energy (SAFE), CH-1864 Vers l'Eglise, Switzerland
[2]Laboratorio Nacional de Fusión, CIEMAT, 28040 Madrid, Spain
[3]Ecole Polytechnique Fédérale de Lausanne (EPFL), Centre de Recherches en Physique des Plasmas (CRPP), Lausanne, CH-1015 Lausanne, Switzerland
[4]Max Planck Institut für Plasmaphysik, Teilinstitut Greifswald, Greifswald, Germany

Email contact main author: wilfred.cooper@epfl.ch

Abstract

The relaxation of the constraint of periodicity imposed by the external confining magnetic field coils in a nominally 4-field period Helias Advanced Stellarator configuration produces weak periodicity-breaking deformations of the plasma. The corrugations are driven by the interaction of the pressure gradient with the magnetic field line curvature and correspond to saturated ideal magnetohydrodynamic interchanges with a mode structure dominated by nonresonant $m = 1, n = \pm 1$ Fourier components. Similar low order mode number oscillations are observed in the 4-field period TJ-II Heliac stellarator [Alejaldre *et al.*, Fusion Technol. **17** 131 (1990)]. The conditions of quasi-isodynamicity of the Helias reactor system investigated are not significantly altered by the periodicity-breaking distortions.

1. INTRODUCTION

Magnetohydrodynamic (MHD) activity can alter the symmetry properties of magnetically confined plasma. A three-dimensional (3D) equilibrium solver [1] has been applied to model the breaking of the axisymmetric properties first in Reversed Field Pinches [2, 3, 4] and more recently in tokamaks [5, 6, 7, 8]. In particular, three-dimensional (3D) internal helical core structures have been previously calculated using the VMEC and the ANIMEC codes that correspond to saturated ideal kink modes that model *snakes* and Long Lived Modes [9] under tokamak hybrid scenario conditions [5, 10].

In stellarator experiments, very long-lasting oscillations characterized by lowest order toroidal and poloidal mode numbers have been detected in many devices like the TJ-II Heliac [11] and the Large Helical Device (LHD) [12]. Previous theoretical and simulation research related to this subject include nonlinear resistive MHD computations of the LHD device that yield saturated solutions [13], and fixed boundary internal nonlinearly MHD stable 2-field period quasiaxisymmetric stellarator configurations have been calculated with the NSTAB code [14]. The deformations in the latter work retain the underlying 2-fold periodicity of the device proposed.

In this work, 3D free boundary ideal magnetohydrodynamic (MHD) equilibrium states are presented for the first time with the VMEC code [1] that develop visible edge distortions that break the periodicity imposed by the coil system in a nominally 4-field period Helias reactor device. We contend that the deformations observed constitute nonlinear saturated ideal magnetohydrodynamic (MHD) interchange structures with low toroidal mode number n driven by the interaction of the pressure gradient with the magnetic field line curvature. The Helias Advanced Stellarator concept investigated displays quasi-isodynamic properties [15, 16], which are essentially unaltered by the periodicity-breaking distortions at reactor-relevant values of $\langle\beta\rangle$. Quasi-isodynamicity corresponds to the condition that particle orbits remain closely linked to their birth flux surfaces, hence we anticipate that fast particle confinement is unaffected by relaxation of the periodicity constraint.

2. THE 3D MHD EQUILIBRIUM STATE

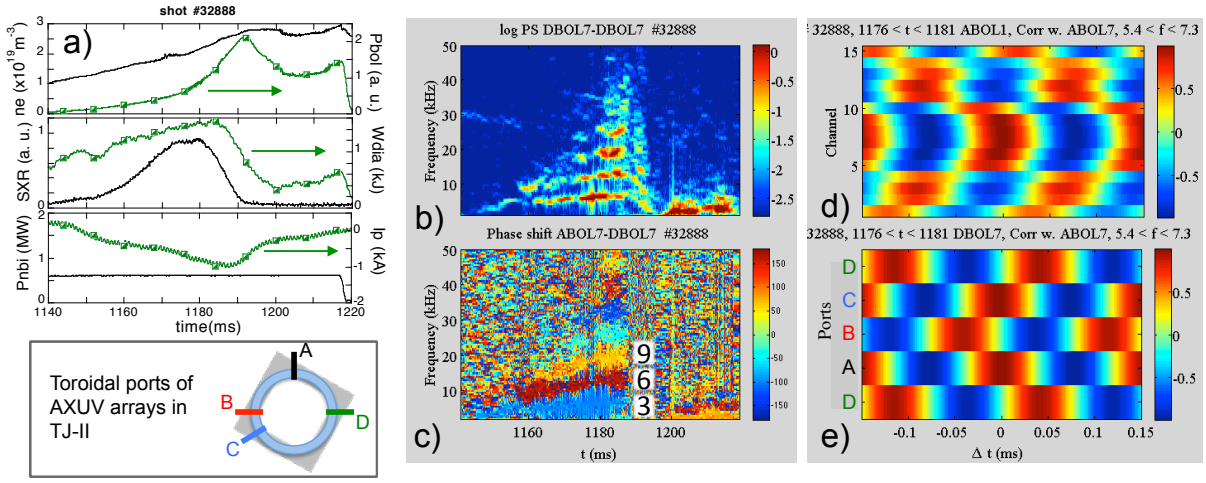

FIG. 1: a) Time traces of TJ-II shot #32888, heated with counter-NBI (core temperatures $T_{e0} \approx 200$ eV, $T_{i0} \approx 100$ eV, not shown) and top-view scheme showing the toroidal location of the radiation arrays. b) Spectrogram of a central radiation chord signal (DBOL7 @ $\rho \approx 0.1$). c) Phase of coherence of the different oscillations determined from equivalent chords measurements separated $\pi/2$ toroidally (sectors D and A). d) Poloidal correlation of one reference channel (ABOL7 @ $\rho \approx 0.1$) with all poloidal chord signals of bolometer array A for the ≈ 6 kHz mode. e) Toroidal correlation of equivalent chords (@ $\rho \approx 0.1$) from each array with the reference channel ABOL7. The labels in c) correspond to the toroidal mode numbers resolved with the four-sectors bolometry system.

2.1 Experimental data with toroidal periodicity breaking in TJ-II plasmas

Long-lasting coherent mode structures have been reported in the TJ-II stellarator [11] and many other toroidal devices [17, 18, 19, 20, 21]. In particular, these oscillations in TJ-II plasmas heated with NBI are typically of very low frequency (4 kHz $\lesssim f \lesssim$ 15 kHz) and last for many confinement times, eventually for the whole length of the discharge. An example of the evolution of the spectrum of modes in this stellarator is displayed in Fig. 1. Provided that the frequency is low, toroidal mode numbers can be resolved according to the relative phase of the modes detected with three AXUV arrays located at sectors separated $\pi/2$ toroidally plus another array located at a fraction of this (see scheme in Fig. 1) [22]. For low enough poloidal mode numbers $m < 7$, the poloidal chords allow for the identification of m-values compatible with resonant values of the rotational transform. In this example, the ≈ 6 kHz mode is seen as an even poloidal structure compatible with $m = 2$, and the apparent phase shifts of this oscillation detected at the four toroidal ports correspond to those expected for an $n = 3$ toroidal mode. Although not shown here, analogous diagrams clearly resolve the toroidal mode numbers of the 12 and 18 kHz modes as 6 and 9, respectively, and the parity of the poloidal numbers. As generally the modes are rather core localized, only in a few cases, mostly $(n, m) = (3, 2)$ and $(n, m) = (5, 3)$, can be also detected with magnetic pick-up coils. The toroidal mode numbers evidence that the mode structures are non-natural, i.e., the oscillations with toroidal mode number that are not an integer multiple of 4 necessarily break the periodicity imposed by the TJ-II coils set. Therefore, even if these modes have their origin in small error magnetic fields that must be fixed in space, the ease with which they rotate in these low pressure (β) plasmas suggests that their existence might be recovered with MHD equilibrium simulations. This provides the motivation to theoretically model this activity and provide physical grounds for the phenomena observed.

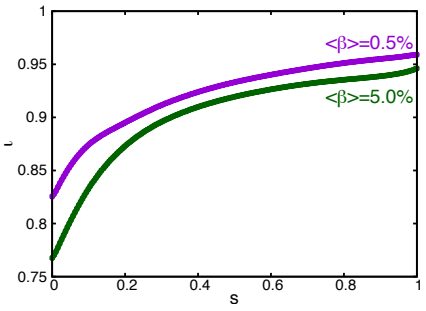

FIG. 2: The rotational transform profiles in a nominally 4-field period Helias reactor configuration at $\langle\beta\rangle = 0.5\%$ and $\langle\beta\rangle = 5\%$ in which the periodicity imposed by the coils is not enforced.

2.2 MHD calculations

Computation of 3D MHD equilibrium states with the VMEC code imposes nested magnetic flux surfaces [1]. The states that are computed represent ideal magnetohydrodynamics because the model precludes magnetic field lines breaking and reconnecting. We have decided to simulate a Helias reactor configuration with a coil system that dictates 4-field periods around the torus because the spectrum of modes required to obtain converged equilibrium solutions is much narrower than that for the 4-field period TJ-II Heliac. This makes the problem more tractable to address. Furthermore, the Helias configuration represents one of the more attractive options for nuclear power production based on the stellarator concept. The plasma energy is given by

$$\mu_0 W = \iiint d^3x \left[\frac{B^2}{2} + \frac{\mu_0 p(s)}{\Gamma - 1}\right], \tag{1}$$

where $\boldsymbol{B}$ is the magnetic field, $p(s)$ is the plasma pressure as a function of the radial variable s ($0 \le s \le 1$), which is proportional to the enclosed toroidal magnetic flux function Φ, and Γ is the adiabatic index. The equilibrium state is obtained by varying the energy functional Eq. 1 with respect to an artificial time variable employing a steepest descent energy minimisation scheme. A Green's function technique is applied to evolve the plasma-vacuum interface to obtain free boundary MHD equilibria where the vacuum magnetic fields are calculated using Biot-Savart's Law from all toroidal and poloidal field coils discretised into finite sized filaments. In free boundary mode, initial guesses for the Fourier amplitudes of R (the distance from the major axis) and Z (the height above the midplane) at the magnetic axis and at the last closed magnetic flux surface (LCFS) must be provided. Though the coil set dictates 4-fold periodicity around the torus, we relax this constraint to include all toroidal mode numbers in the range $-20 \le n \le 20$ and poloidal mode numbers $0 \le m \le 11$. Typically, the 4-fold periodic Fourier components of $R \equiv \sum_{m,n} R_{m,n} \cos(m\theta - n\phi)$ and $Z \equiv \sum_{m,n} Z_{m,n} \sin(m\theta - n\phi)$ (stellarator symmetry is assumed) at the plasma-vacuum interface are chosen as $R_{0,0} = 17.7$, $R_{0,4} = 0.72$, $R_{1,0} = 2.15$, $R_{1,4} = 0.99$, $Z_{0,0} = 0$, $Z_{0,4} = 0.33$, $R_{1,0} = 2.448$, $Z_{1,4} = 1.33$ (dimensions in m). Initial edge periodicity-breaking components are prescribed through the parameter δ_i, such that $R_{1,1} = Z_{1,1} = \delta_i$ and $R_{1,-1} = Z_{1,-1} = -\delta_i$.

All calculations performed in this article have vanishing toroidal current within each flux surface $2\pi J(s) = 0$ and pressure profile prescribed as $p(s) = p(0)(1-s)(1-s^4)$. The rotational transform profiles $\iota(s)$ for the Helias reactor configuration examined at $\langle\beta\rangle = 0.5\%$ and $\langle\beta\rangle = 5\%$ are plotted as a function of s in Fig. 2. Note that $\iota = 1$ is outside the plasma; the main low order resonances that break the 4-fold periodicity of the coils are $n/m = 10/11$, $9/10$, $7/8$, $6/7$ and $5/6$.

The shape of the LCFS for the Helias reactor system under consideration at each of the eggplant cross sections throughout one toroidal transit are projected onto one plane in Fig. 3 at $\langle\beta\rangle = 0.5\%$, 2% and 4%. There are visible deformations of the LCFS in this range of $\langle\beta\rangle$ values.

The Plasma-Vacuum Interface shape at the bean, eggplant and triangular cross sections over 1 toroidal transit at $\langle\beta\rangle = 5.6\%$ shows the small corrugation of the edge surface at each superimposed plane in Fig. 4. The mid plane pressure distribution through a full toroidal transit ($0 \le \phi \le 2\pi$) at $\langle\beta\rangle = 5\%$ is

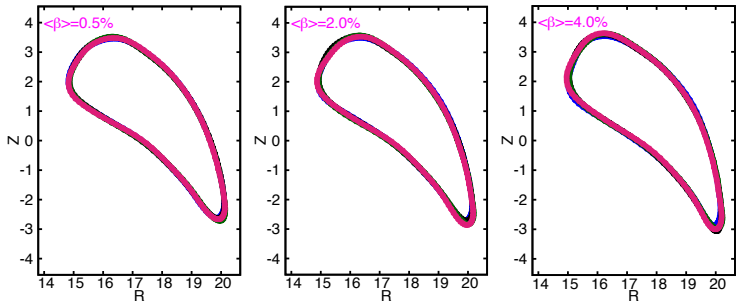

FIG. 3: The superimposed shape of the LCFS at the 4 eggplant cross sections at $\langle\beta\rangle = 0.5\%$ (left), at 2.0% (middle) and at 4.0% (right) in a Helias reactor system. The superimposed shapes match exactly when the 4-fold coil periodicity constraint is imposed.

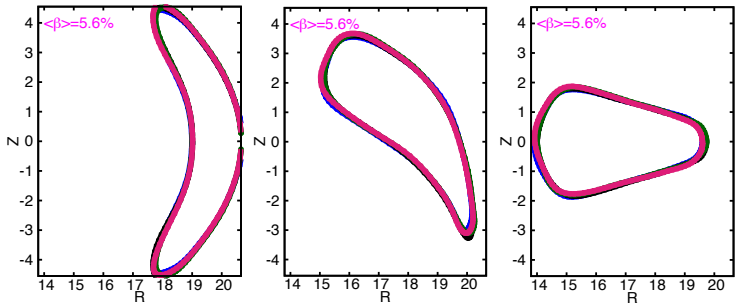

FIG. 4: The superimposed shapes of the LCFS at $\langle\beta\rangle = 5.6\%$ at the bean-shaped cross section (left), at the eggplant cross section (middle) and at the triangular cross section (right) in a Helias reactor configuration. The 4 superimposed shapes match exactly at each of the cross sections when the 4-fold coil periodicity constraint is imposed.

presented in Fig. 5. It shows that the bulk plasma retains the underlying 4-fold periodicity of the system. However, near the plasma boundary the inner and outer edge positions are slightly displaced from one period to the next confirming a small $n = 1$ modulation.

Eddy currents in the surrounding metallic walls produce periodicity-breaking perturbations that can also be enhanced by linear MHD instability dynamics (the system investigated is unstable to linear ideal MHD modes when $\langle\beta\rangle$ exceeds 0.6%). This justifies increasing δ_i with $\langle\beta\rangle$. Fig. 6 (a) shows the variation of the volume average total energy $\left\langle\left\langle p + B^2/(2\mu_0)\right\rangle\right\rangle$ within the plasma as a function of the parameter δ_i that shows that the minimum energy state is achieved for $\delta_i = 0.31$ m. For lower $\langle\beta\rangle$, the energetically favoured MHD equilibrium solutions are achieved with progressively lower values of the initial distortion δ_i prescribed at the plasma boundary. We define $\langle\langle\mathcal{A}\rangle\rangle \equiv \int d^3x\mathcal{A}/\int d^3x$.

The minimum energy state in the range $\langle\beta\rangle = 0.5\% - 5.6\%$ is plotted in Fig. 6 (b). The initial guesses for the $m = 1$, $n = \pm 1$ components of R and Z specified by δ_i that yield the minimum energy states at each $\langle\beta\rangle$ are identified in the plot. $\Delta\left\langle\left\langle p + B^2/(2\mu_0)\right\rangle\right\rangle$ corresponds to the difference between $\left\langle\left\langle p + B^2/(2\mu_0)\right\rangle\right\rangle$ evaluated at finite δ_i and $\delta_i = 0$. Note that the ordinate values in Fig. 6 (b) are negative indicating that the volume averaged total plasma energy obtained at the finite values of δ_i is lower than that for $\delta_i = 0$ in the range of $\langle\beta\rangle$ explored.

A Fourier decomposition of R at the outermost magnetic flux surface is undertaken and displayed in Fig. 7 at $\langle\beta\rangle = 0.5\%$ and 5.0%. In this figure we limit the periodicity-breaking components to the range $0 \le m \le 4$ and $-13 \le n \le 13$ because they have significant amplitudes only for relatively low mode numbers m, n. Hence we would like to highlight that the main resonances identified in the description of Fig. 2 that break the periodicity of the system provide only weak distortions compared with the mainly non-resonant contributions of $R_{m,n}$ that appear in Fig. 7. The spectrum is slightly broader and the amplitudes smaller in absolute magnitude at the lower $\langle\beta\rangle$ values. Though the amplitudes of the $R_{1,\pm1}$

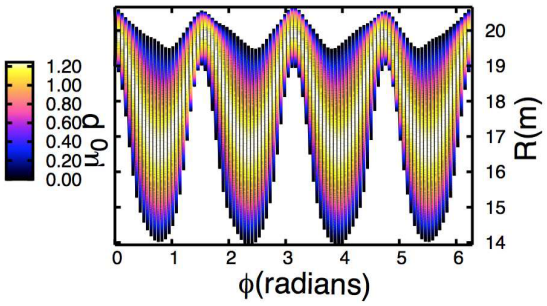

FIG. 5: The pressure distribution $\mu_0 p$ (in units of Pa×H/m*) at the mid-plane as a function of the toroidal angle ϕ and the distance from the major axis R for the Helias reactor minimum energy equilibrium state at $\langle\beta\rangle = 5\%$.*

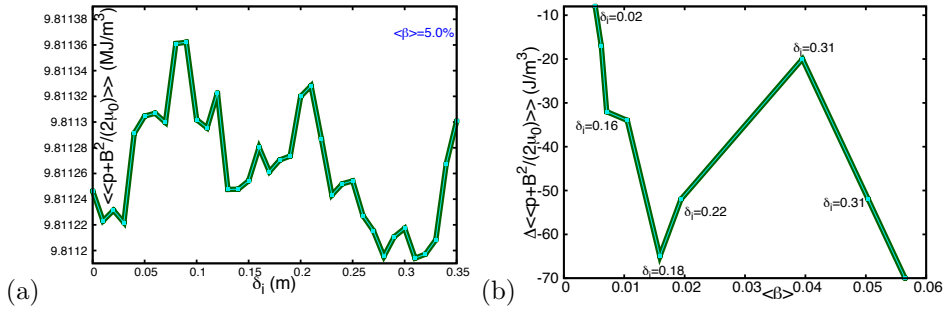

FIG. 6: Left: The value of the volume averaged total plasma energy $\langle\langle p + B^2/(2\mu_0)\rangle\rangle$ at the minimum energy state as a function of the initial guess of the distortion δ_i in a Helias reactor system at $\langle\beta\rangle = 5.0\%$. The initial Fourier amplitudes of R and Z corresponding to the $m = 1, n = \pm 1$ components are $R_{1,1} = Z_{1,1} = -R_{1,-1} = -Z_{1,-1} = \delta_i$. Right: The value of the difference of the volume averaged total plasma energy $\langle\langle p + B^2/(2\mu_0)\rangle\rangle$ at finite δ_i (which corresponds to the minimum energy state) with that at $\delta_i = 0$ as a function of $\langle\beta\rangle$. The values of δ_i are labelled at each value of $\langle\beta\rangle$ plotted.

term increase in magnitude with $\langle\beta\rangle$, the resulting interference pattern appears not to be constructive as the corrugations of the shape of the last surface as shown in figures 3 and 4 do not change much.

In order to further illustrate the dominance of the low-mode numbers in the periodicity-breaking components, we show the Fourier decomposition of Z in figure 8 (left) in the whole modal plane. In addition, in figure 8 (right) we find that the spectrum of significant Fourier components of the magnetic field strength B is relatively broader compared with the geometric corrugations, but still limited to low m and n (typically $0 \leq m \leq 4$, $-2 \leq n \leq 12$ at $\langle\beta\rangle = 5\%$).

In current-free stellarators, the interaction of the pressure gradient with the magnetic field line curvature constitutes the principal driving mechanism for MHD instabilities. The structure of $2\sqrt{g}p'(s)\boldsymbol{\kappa}\cdot\boldsymbol{\nabla}s$ on a flux surface close to the edge of the plasma reveals that the most destabilising contribution (most negative) concentrates near the outside edge of one of the bean-shaped cross sections indicating an important $n = 1$ distortion. Furthermore, the structure when the 4-fold periodicity is relaxed is more closely magnetic field aligned compared with the 4-field period constrained configuration where it is cross-field aligned. The comparison between the 2 cases at $\langle\beta\rangle = 5\%$ is presented in Fig. 9. Another important observation is that the range of values for $2\sqrt{g}p'(s)\boldsymbol{\kappa}\cdot\boldsymbol{\nabla}s$ is neutral (with respect to positive and negative values) when the periodicity constraint is relaxed indicating marginal stability. However, it tends to be more negative when the 4-fold periodicity is enforced suggesting that this configuration is linearly unstable to ideal MHD, a condition we have confirmed with the TERPSICHORE code [23, 24]. The periodicity-breaking deformations constitute a saturated ideal MHD instability state.

The Helias reactor configuration examined approaches conditions of quasi-isodynamicity [15, 16]. The poloidal closure of the contours of the 2^{nd} adiabatic invariant $\mathcal{J}$ in a polar plot for particles with pitch

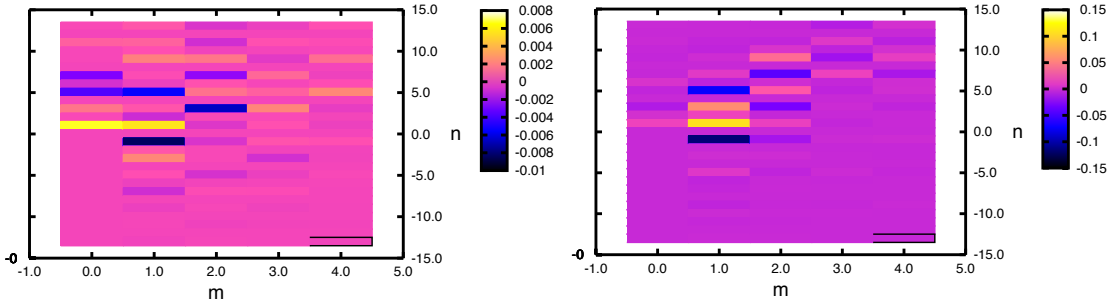

FIG. 7: The dominant Fourier components of R on the LCFS in a Helias reactor system at the minimum energy state at $\langle\beta\rangle = 0.5\%$ (left) and $\langle\beta\rangle = 5.0\%$ (right) poloidal mode number m and toroidal mode number n phase space. To visualize the periodicity-breaking Fourier terms, the dominant 4-fold periodic components of R are suppressed. The main periodicity-breaking terms have significant amplitude for relatively low m, n values. Consequently, we limit the display to the range $0 \leq m \leq 4$ and $-13 \leq n \leq 13$. The Fourier amplitudes $R_{m,n}$ are normalized to the $R_{1,0}$ term.

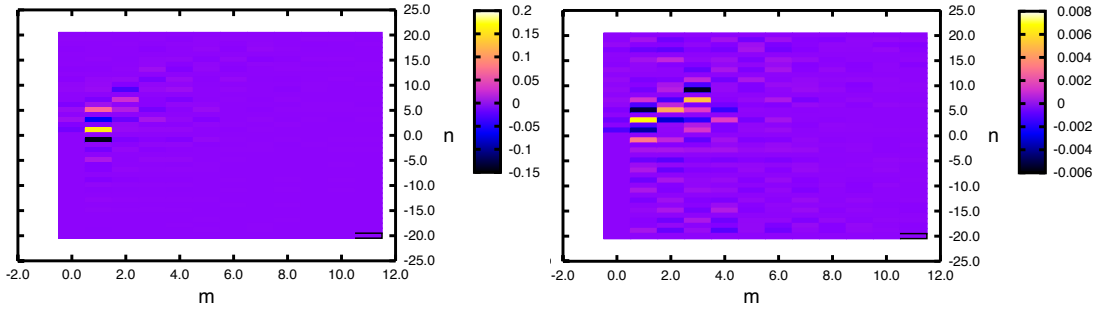

FIG. 8: Complete spectrum, $0 \leq m \leq 11$ and $-20 \leq n \leq 20$, of the Fourier decomposition of Z (left) and the magnetic field B (right) on the LCFS for the calculation at $\langle\beta\rangle = 5\%$. See Fig. 7.

angles that vary from deeply to barely trapped represents a good measure of the confinement of fast ions and of neoclassical transport properties in general. We have found that the relaxation of the periodicity exacted by the external coils does not modify in a significant way the contours of the $\mathcal{J}$ for different particle pitch angles. A comparison of the $\mathcal{J}$ behavior for the general equilibrium case and the 4-fold periodic case at $\langle\beta\rangle = 5\%$ demonstrates that both are very similar, as shown in Fig. 10. Thus energetic particle confinement and neoclassical transport should not be seriously impacted whether periodicity is enforced or not.

3. SUMMARY AND CONCLUSIONS

In summary, long-lived low frequency oscillations with toroidal mode number smaller than the machine periodicity have been detected in stellarator system such as TJ-II. We report, for the first time, free boundary stellarator equilibria using the VMEC code with novel 3D distortions to the plasma-vacuum interface that break the underlying periodicity imposed by the external magnetic confinement coils of a nominally 4-field period Helias reactor. The edge corrugations occur in the range $0.5\% < \langle\beta\rangle < 5.6\%$ investigated. The Fourier spectrum of R and Z at the LCFS is dominantly $m = 1$, $n = \pm 1$ at $\langle\beta\rangle = 5\%$. The $m/n = 1/\pm 1$ structures are nonresonant as $\iota_{max} < 0.95$. We contend that these geometric deformations correspond to saturated ideal MHD interchanges driven by the interaction of the pressure gradient with the magnetic field curvature. The $2\sqrt{g}p'(s)\boldsymbol{\kappa} \cdot \boldsymbol{\nabla} s$ structure confirms a $n = 1$ modulation around the torus. The quasi-isodynamic properties of the Helias configuration we have investigated are not significantly altered by the periodicity-breaking corrugations we report, thus we surmise that fast particle confinement and neoclassical transport will not be affected. The edge distortions are very benign (even at high $\langle\beta\rangle > 5\%$) compared with other confinement concepts. These conditions augur very

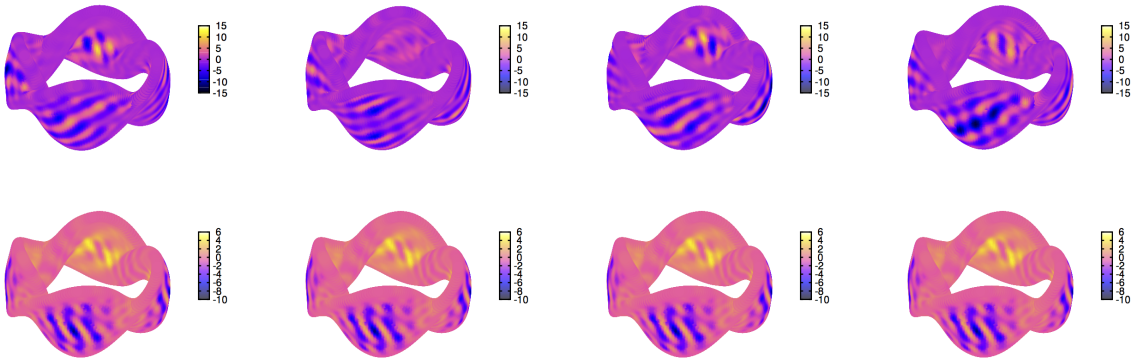

FIG. 9: The distribution of the interaction of the pressure gradient with the magnetic field line curvature $2\sqrt{g}p'(s)\boldsymbol{\kappa}\cdot\boldsymbol{\nabla}s$ *on a magnetic flux surface close to the edge of the plasma at* $\langle\beta\rangle = 5\%$*. The top row represents the equilibrium state with unconstrained periodicity. The bottom row represents the equilibrium state constrained to satisfy the* 4*-fold periodicity of the coils.*

favorably for the Helias advanced stellarator system as a power producing fusion energy reactor concept.

The simulation model we have applied constrains the magnetic surfaces to remain nested. Our work thus opens new avenues of research like the consideration of more general equilibrium approaches that allow for the formation of periodicity-breaking magnetic islands and internal stochastic regions [25, 26, 27] (typically these solvers use a VMEC solution as an initial guess). Also, nonlinear kinetic theory can be invoked to examine the generation of finite frequency oscillations using the VMEC equilibria we have computed. Some complementary simulations related to this research appear in Ref. [28].

ACKNOWLEDGEMENTS

The work was partially supported by the Swiss National Science Foundation and by the Spanish Government (project ENE2014-52174-P and grant FIS2017-85252-R). This work has been carried out within the framework of the EUROfusion Consortium and has received funding from the Euratom research and training programme 2014–2018 under grant agreement No. 633053. The views and opinions expressed herein do not necessarily reflect those of the European Commission. We thank Dr. S. P. Hirshman for providing us with the VMEC code, Dr. M. Drevlak for using routines of the ROSE code, Dr. H. F. G. Wobig (RIP) and Dr. J. Kisslinger for the Helias coils.

REFERENCES

[1] HIRSHMAN, S.P., et al., Comput. Phys. Commun. **43** (1986) 143.
[2] LORENZINI, R., et al., Nature Physics **5** 570–574 (2009)
[3] TERRANOVA, D., et al, Plasma Phys. Control. Fusion **52** (2010) 124023.
[4] HANSON, J.D., et al., Nucl. Fusion **53** (2013) 083016.
[5] COOPER, W.A., et al, Phys. Rev. Lett. **105** (2010) 035003 .
[6] COOPER, W.A., et al, Nucl. Fusion **53** (2013) 073021.
[7] COOPER, W.A., et al, Phys. Plasmas **23** (2016) 040701.
[8] WINGEN, A., et al., Nucl. Fusion **56** (2016) 016013.
[9] CHAPMAN, I.T., et al., Nucl. Fusion **50** (2010) 045007.
[10] COOPER, W.A., et al., Nucl. Fusion **51** (2011) 072002.
[11] OCHANDO, M.A., et al, in Procs. 42^{nd} EPS Conf. Plasma Phys., Lisbon, Portugal, 2015.
[12] TAKEMURA, Y., et al, Nucl. Fusion **52** (2012) 102001.

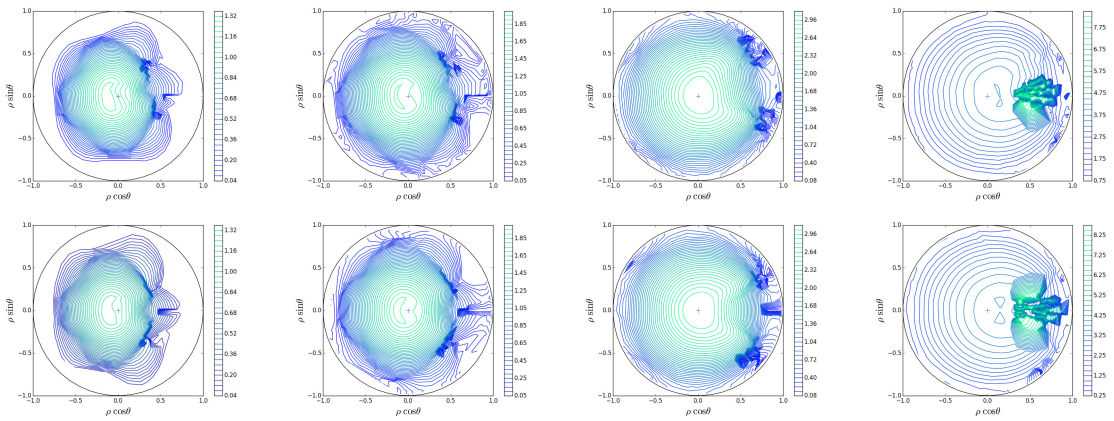

FIG. 10: The contours of the second adiabatic invariant $\mathcal{J}$ in polar coordinate representation for a Helias reactor configuration at $\langle\beta\rangle = 5\%$. The radial variable is $\rho = \sqrt{s}$ and θ is the poloidal angle. The columns correspond to reference magnetic field values $B_{\rm ref} = 4.55$ T, 4.6 T, 4.7 T and 4.8 T from left to right, respectively. The particle pitch angle correspond to $\lambda \equiv \mu/\mathcal{E} = 1/B_{\rm ref}$. The top row represents the equilibrium state with unconstrained periodicity. The bottom row represents the equilibrium state constrained to satisfy the 4-fold periodicity of the coils.

[13] ICHIGUCHI, K., et al., Nucl. Fusion **43** (2003) 1101.
[14] GARABEDIAN, P., Proc. Natl. Acad. Sci. USA **103** (2006) 19232–19236.
[15] NÜHRENBERG, J., Plasma Phys. Control. Fusion **52**, 124003 (2010).
[16] MYNICK, H., Phys. Plasmas **13** (2006) 058102.
[17] HARRIS, J.H., et al., Phys. Rev. Lett. **53** (1984) 2242.
[18] MANICKAM, J., et al., Nucl. Fusion **27** (1987) 1461.
[19] GRYAZNEVICH, M.P., et al., Nucl. Fusion **48** (2008) 084003.
[20] DELGADO-APARICIO, L.F., et al., Nucl. Fusion **53** (2013) 043019.
[21] ZHANG, R-B., et al., Plasma Phys. Control. Fusion **56** (2014) 095007.
[22] OCHANDO, M.A., et al., Fusion Sci. Technol. **50** (2006) 313.
[23] ANDERSON, D.V., et al., Int. J. Supercomp. Appl. **4** (1990) 34.
[24] COOPER, W.A., Plasma Phys. Control. Fusion **34** 1011 (1992).
[25] SUZUKI, Y., Nucl. Fusion **46** (2006) L19.
[26] PERAZA-RODRIGUEZ, H., et al., Phys. Plasmas **24** (2017) 082516.
[27] LOIZU, J., et al., Phys. Plasmas **23** (2016) 112505.
[28] COOPER, W.A., et al., Nucl. Fusion **58** (2018) 124002.